

Structure of steps on As-passivated Si(111): *Ab initio* calculations and scanning tunneling microscopy

A. Antons,¹ R. Berger,¹ K. Schroeder,¹ and B. Voigtländer²

¹*Institut für Festkörperforschung, Forschungszentrum Jülich, D-52425 Jülich, Germany*

²*Institut für Schichten und Grenzflächen and Center of Nanoelectronic Systems for Information Technology, Forschungszentrum Jülich, D-52425 Jülich, Germany*

(Received 6 September 2005; revised manuscript received 31 January 2006; published 21 March 2006)

The structures of terrace steps on As-covered Si(111) are examined using *ab initio* calculations. In scanning tunneling microscope (STM) images, two orientations of steps are found to terminate As-covered Si islands after annealing: $[11\bar{2}]$ and $[\bar{1}\bar{1}2]$. Total energy calculations and simulations of STM images yield detailed information on the atomic structures of the steps: In the lowest-energy configuration for both orientations, surplus As atoms replace any exposed Si atoms at the steps. The As atoms rearrange to establish a threefold coordination. For $[11\bar{2}]$ steps the atom positions of the relaxed configuration are very close to the ideal bulk positions, but for $[\bar{1}\bar{1}2]$ steps the terminating As atoms form dimers in front of the steps. The different atomic structures of the two step orientations clearly show up in the simulated STM images for negative bias (occupied states imaged), the STM images for positive bias (unoccupied states) are much less distinctive. All features of existing experimental positive-bias STM images can be explained by an analysis of the electronic local density of states. With the calculated step energies we construct a phase diagram for the equilibrium shape of As-covered islands. In the accessible range of As chemical potentials between As bulk and As₄ molecules, we expect either triangular islands terminated by $[11\bar{2}]$ steps or hexagons with long edges of $[11\bar{2}]$ orientation and short ones with $[\bar{1}\bar{1}2]$ orientation.

DOI: [10.1103/PhysRevB.73.125327](https://doi.org/10.1103/PhysRevB.73.125327)

PACS number(s): 68.35.-p, 68.55.-a, 68.43.Bc, 68.37.Ef

I. INTRODUCTION

New design of semiconductor devices (transistors, lasers) often requires the growth of atomically flat layered heterostructures.^{1,2} Due to lattice mismatch this is not easily realized. An important example is the Ge/Si-heterostructure whose lattice constants differ by $\approx 4\%$. After the pioneering work of Copel *et al.*³ on surfactant-mediated layer-by-layer growth of Ge on Si, much effort has been devoted to the optimization and understanding of the microscopic mechanism of the so-called *surfactant effect*.⁴ Whereas on the clean Si(111) surface Ge grows in the Stranski-Krastanov mode forming large three-dimensional islands, with an overlayer of As, Sb, or Bi one finds layer-by-layer growth on Si(111) and Si(001) surfaces.^{3,5-8} A metal oxide semiconductor field-effect transistor structure with an active layer of *p*-type Ge has been grown successfully on a Si(111) substrate using a Sb surfactant layer.⁹ With a surfactant layer the nucleation of islands and their growth during epitaxy is determined by the competition between diffusion of the adatoms on top of the surfactant layer and the incorporation by an exchange reaction with a surfactant atom. On a surface with terrace steps or in a situation with developed islands, the incorporation at the step edges is an additional competing process. While the kinetics of single adatoms on flat terraces as well as the sequence of clustering on the Si(111) surface covered with different surfactants have been clarified to a large extent,¹⁰⁻¹⁴ long-time growth simulations¹⁵⁻¹⁷ using kinetic Monte-Carlo methods show that the incorporation barriers at surfactant covered step edges play a decisive role in understanding the competing processes of step flow growth and nucleation of islands. To obtain growth by island nucleation on the flat

terraces, as observed in experiment, Kaxiras and co-workers have postulated that the step edges on Si(111) are passivated by group-V atoms just as the terraces are.

Steps on surfaces are studied because of their relevance for film growth. A recent study of Si self-assembly at steps on clean Si(111) 7×7 ,^{18,19} shows a temperature dependence of the step-induced structures: Growth temperatures below 300 °C lead to Si atomic wires parallel to the steps, whereas at temperatures above 400 °C, a periodic arrangement of Si clusters along the steps is observed. The stability of steps on the clean Si(111) 2×1 has been investigated.²⁰ The results reveal that the Si atoms at the step edge rebind to reduce the number of dangling bonds. Thus, it can be expected that the attachment of foreign atoms to the steps changes the step structure. The attachment of deposited atoms on vicinal surfaces has been analyzed in recent studies motivated by the search for atomic wires. Experiments and density-functional-based calculations have been performed for Au wires on Si(557).²¹⁻²⁴ The Au atoms arrange in a wire parallel to the steps, but not close to the step edge, as one would naively assume. The Au wire is placed in the middle of the (111) terrace and the surface Si atoms arrange in a peculiar way in order to minimize the number of dangling bonds. The minimal energy structure obtained by density-functional calculations is in good agreement with the one deduced from x-ray studies²³ as well as with the scanning tunneling microscope (STM) images from Ref. 22. The theoretical STM simulations suggest that the most prominent features are due to chains of Si adatoms and not due to the Au atoms, as was previously assumed. From the results of a study of Ga adsorption on Si(112), the authors^{25,26} conclude that bond saturation on the terrace as well as at the steps is important for

energy reduction of the structure. In fact, the resulting structure shows a 6×1 superstructure unit cell with ten Ga atoms arranged in a zig-zag double chain, and two aligned vacancies. The importance of step decoration for metal wire growth on Si surfaces is thus questionable, at least for Au and Ga.

Group-V surfactant layers have been shown to change the surface structure of Si(111): For 1 monolayer (ML) As, an unreconstructed bulk termination is found with a (1×1) hexagonal surface unit cell, and the As atoms constitute the outer layer of the terminating double layer.²⁷ On the other hand, for 1 ML Sb and Bi, a $(\sqrt{3} \times \sqrt{3})$ hexagonal surface unit cell is found, and the Sb or Bi atoms form trimers (centered at the sites of the second Si layer) on top of a Si double layer.^{28,29} No detailed study of the step structure on group-V-covered Si(111) has been performed. We chose the case of As on Si(111) because As is a widely used dopant in Si, and is a frequently used surfactant in epitaxial growth.³

In this work we will present the results of *ab initio* calculations for the structures and energies of the $[11\bar{2}]$ - and $[\bar{1}\bar{1}2]$ -oriented step edges, which are most commonly found to terminate Si islands grown by homoepitaxy on As-covered Si(111).¹⁰ To connect to experiment, simulated and experimental STM images for the most stable step configurations will be discussed. The following questions will be addressed in detail: (i) What is the equilibrium structure of step edges on As-covered Si(111)? (ii) Where are As atoms attached at terrace steps on Si(111)? (iii) Is the assumption correct that surfactants not only passivate the flat surface but also the step edges, thus reducing the incorporation probability of adatoms? (iv) What is the equilibrium shape of Si islands on As-covered Si(111)?

II. EXPERIMENTS

Positive-bias STM imaging (where electrons are tunneling from the STM tip to the unoccupied states of the sample) have been performed. The islands developed during As deposition on the clean (7×7) Si(111) surface at 975 K. An effusion cell was used to evaporate As. To reach the saturation coverage of one monolayer As, we offer access As (5×10^{-8} mbar pressure in the chamber) for several minutes. During the process of Si-island formation, the deposition of access As provides an As-saturated surface at any time. After the furnace was shut off, the sample temperature was lowered to 775 K until the pressure in the chamber (induced by As) was below 10^{-9} mbar.

During the change of the reconstruction from the initial (7×7) structure to the As covered (1×1) structure in which As substitutes the upper part of the Si bilayer, Si atoms of the upper layers were available for island growth. The surface showed triangular and hexagonal islands terminated by steps with $[11\bar{2}]$ and/or $[\bar{1}\bar{1}2]$ orientation. A representative positive-bias STM image is shown in Fig. 1. Two steps with $[\bar{1}\bar{1}2]$ orientation run diagonally through the image. The step edges of the smaller triangular islands have mostly $[11\bar{2}]$ orientation, while on the larger hexagonal islands the longer

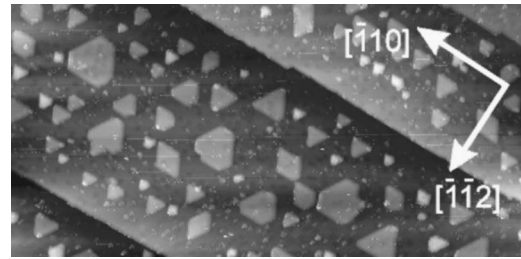


FIG. 1. STM image of islands on an As-covered Si(111) surface, showing triangular and irregular hexagonal islands terminated by steps with $[11\bar{2}]$ and/or $[\bar{1}\bar{1}2]$ orientation. Image width: 1500 Å, sample bias voltage: +2 V. The two long steps terminating the terrace have $[\bar{1}\bar{1}2]$ orientation.

step edges have $[\bar{1}\bar{1}2]$ orientation. The orientation of the steps has been determined by using the orientation of the unit cell on the clean (7×7) Si(111) surface as a reference: the vector connecting the faulted part with the unfaulted part lies in the $[11\bar{2}]$ direction.³⁰

From the STM images, and in particular from the enlarged image of a single triangular island (Fig. 2), the following features of Si islands covered with As can be identified: (i) The islands show the same (1×1) surface reconstruction as the terraces. (ii) The height of the islands is one Si(111) double layer. (iii) The island edges show exclusively $[11\bar{2}]$ and $[\bar{1}\bar{1}2]$ orientations. The edges shown in the STM image in Fig. 2 have been assigned to the $[11\bar{2}]$ orientation. (iv) The island edge atoms for both step orientations show up in the STM image as brighter dots compared to the terrace atoms, they appear to be elevated with respect to the island top plane. Unfortunately, neither the atomic arrangement at the island rim, nor the chemical nature of the atoms can be extracted without further input from other methods or from theory.

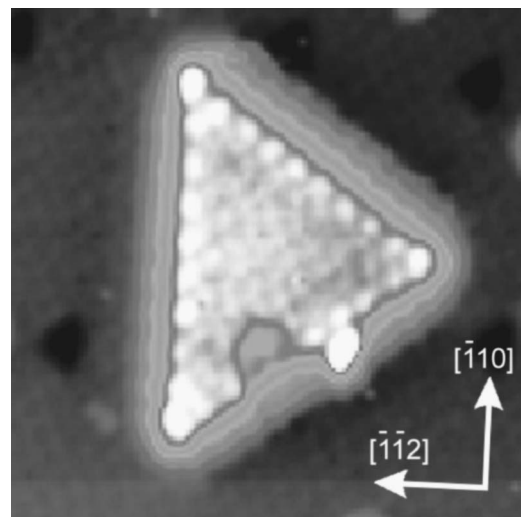


FIG. 2. Positive-bias STM image of a triangular Si island on As-covered Si(111). The edges are oriented in the $[11\bar{2}]$ direction. Image width: 50 Å, sample bias: +1.9 V

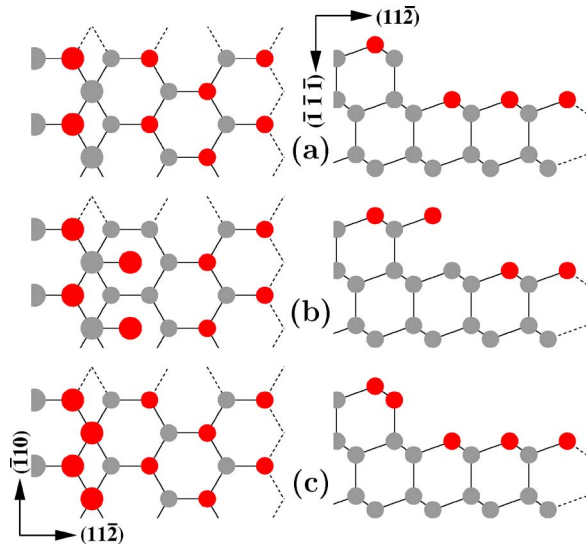


FIG. 3. (Color online) Top view (left) and side view (right) of three different configurations of $[11\bar{2}]$ steps on Si(111):As. Si atoms are light, As atoms dark. (a) Exposed Si at step edge, (b) attached overhanging As atom, and (c) exposed Si replaced by As.

III. MODEL CALCULATIONS

We have performed *ab initio* calculations of structures and total energies of terrace steps for $[11\bar{2}]$ and $[\bar{1}\bar{1}2]$ orientations, taking into consideration three possible terminations of the terrace (see Fig. 3 for $[11\bar{2}]$ steps). Starting from a perfectly (111)-oriented Si surface, the initial step configurations are constructed by cutting away a part of the surface Si double layer, and replacing the exposed Si atoms on the emerging upper and lower terrace by As atoms. The resulting step exhibits an exposed Si atom at the terrace edge, as is shown for the $[11\bar{2}]$ -oriented step in Fig. 3(a). The dangling bond belonging to this Si atom cannot be avoided without reconfiguring the step configurations. The two most likely configurations are shown in Figs. 3(b) and 3(c). One can either attach an additional As atom to the exposed Si, and replace the As atom on the lower terrace closest to the step edge with Si, or replace the exposed Si with As. Both configurations need extra As atoms that have to be provided during island growth. With the growth conditions chosen (see Sec. II), it is clear that plenty of As is available.

A. Calculation details

All calculations have been carried out with our massively parallelized *ab initio* molecular dynamics program EST-COMPP (for details see Ref. 31), using norm-conserving pseudopotentials of the Kleinman-Bylander form³² and the local density approximation.³³ Force calculations combined with molecular statics³⁴ are used to determine the minimum energy configurations. The systems are simulated by a repeated slab model consisting of ten atomic Si(111) layers and 1 ML As on each Si surface in an inversion symmetric arrangement. We use a periodicity length perpendicular to the steps, which yields a terrace width of 4 or 5 nearest-neighbor

TABLE I. Geometrical parameters of unit cells.

Step	Area	Configuration	Si atoms	As atoms	Additional As
$[11\bar{2}]$	$17\frac{1}{3}$ u.c.	Exposed Si	68	16	$-1\frac{1}{3}$
		Overhang As	72	16	$-1\frac{1}{3}$
		Si replaced by As	64	20	$+2\frac{2}{3}$
$[\bar{1}\bar{1}2]$	$14\frac{2}{3}$ u.c.	Exposed Si	68	12	$-2\frac{2}{3}$
		Overhang As	74	12	$-2\frac{2}{3}$
		Si replaced by As	64	20	$+1\frac{1}{3}$

distances. Opposite surfaces are separated by a vacuum equivalent to eight atomic Si layers. We find that two \mathbf{k}_{\parallel} -points in the surface Brillouin-zone and a cutoff energy of 9 Ry in the plane wave basis set yield reliable results.³⁵ The relaxed step configurations are determined by applying symmetry-unrestricted geometry optimization including all atoms except those of eight atoms in the two innermost atomic layers of the slab, starting from ideally bulk-terminated positions for all atoms. To establish minimum energy configurations, we converged the forces acting on the atoms to less than 0.1 mRy/a.u. In order to obtain laterally periodic cells containing one step of a given orientation, it was necessary to use different basis vectors parallel to the surface for the two different step orientations. This yields different numbers of atoms and different surface areas for the two cells which are listed in Table I, the area is in units of the (1×1) lateral unit cell, the number of additional As atoms is calculated relative to the coverage of the (1×1) flat terrace structure. Our unit cells always contain four unit step lengths, since there are two equivalent surfaces and the basis vector along the step has a length of two nearest-neighbor distances.

IV. STEP STRUCTURES AND ENERGIES

In order to calculate the energies in a comparable fashion for systems that contain different numbers of atoms and different surface areas, we have to specify reference configurations. For Si atoms, we have used Si bulk [$E(\text{Si}) = -7.931\,134$ Ry], and for As atoms, As_4 molecules [$(1/4)E(\text{As}_4) = -12.579\,728$ Ry] as one reference and As bulk [$E(\text{As}) = -12.615\,445$ Ry] as a second reference. The energies per unit step length of all calculated step configurations are collected in Table II. The different reference configurations that account for the possible variation of the As chemical potential yield quantitatively different, but qualitatively similar results: The steps with additional As atoms replacing the exposed Si atoms are the lowest-energy configurations for both orientations. Because of their nearly ideal bond structure, steps with $[11\bar{2}]$ orientation are more stable than those with $[\bar{1}\bar{1}2]$ orientation.

One can imagine that the other configurations that we have considered appear (locally) as intermediate stages, when growth proceeds by attachment of Si atoms leading to

TABLE II. Energies per unit length of steps on Si(111):As.

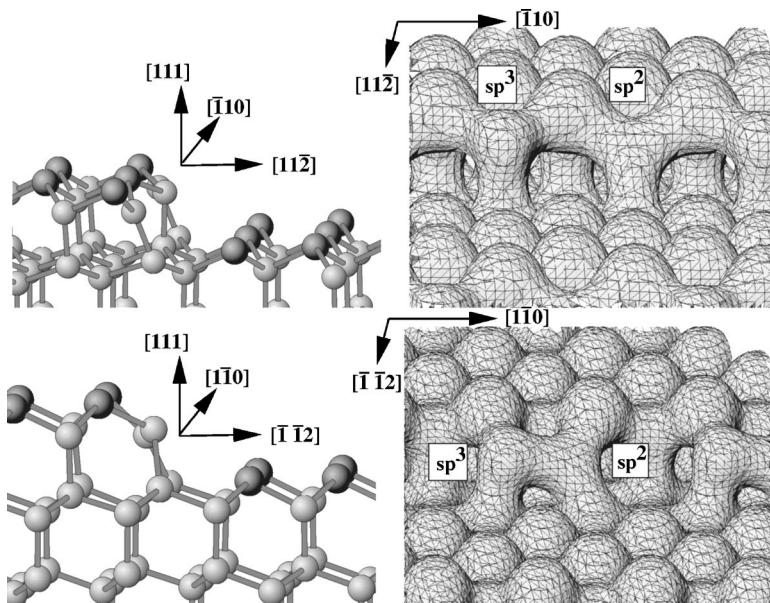
Step	Configuration	Energies [mRy]	
		As ₄ mol ^a	As bulk ^a
[11 $\bar{2}$]	Exposed Si	98.11	86.20
	Overhanging As	133.00	121.09
	Si replaced by As	2.58	26.39
[$\bar{1}\bar{1}2$]	Exposed Si	113.19	89.38
	Overhanging As	114.46	90.65
	Si replaced by As	19.28	31.18

^aReference configuration (see text).

step flow in a two-step procedure: namely, first attaching an additional Si atom to the As-terminated configuration [Fig. 3(c)], and pushing the second-layer edge As atom out, leads to the overhanging-As configuration [Fig. 3(b)], and then secondly replacing the lower-layer As in front of the step edge by a Si atom and pushing the replaced As up to the second layer of the upper terrace, moves the step edge forward by one unit of the As-terminated step [Fig. 3(c)]. In addition, attaching an additional As atom to an overhanging As [Fig. 3(b)] yields one unit of the As-terminated step [Fig. 3(c)]. We have excluded very unlikely configurations right from the beginning; i.e., configurations where dangling bonds would appear that cannot be compensated by atomic relaxations. In the next paragraphs we discuss the relaxed structures of all three initial configurations in detail.

A. Exposed Si atoms

As expected, the relaxed configurations with exposed Si atoms at the step edge deviate strongly from the starting configuration. In Fig. 4, the end configurations of [11 $\bar{2}$] steps (upper panels) and of [$\bar{1}\bar{1}2$] steps (lower panels) are shown.



For the [11 $\bar{2}$] step orientation, the main effect is that the step edge Si atoms buckle: one Si atom retracts into the bulk until it forms a nearly perfect planar triangle with its three nearest neighbors. The analysis of the electronic structure shows a sp^2 -hybrid configuration on this Si atom, and the remaining p_z state is not occupied. The slight reduction of the bond lengths of this atom (98.2% of the Si bulk bond length to the Si neighbor, and 98.6% of the Si bulk bond length to the two As neighbors compared to 104% for the As-Si bond on the flat terrace) is consistent with this picture. The other Si atom shows a nearly perfect tetrahedral configuration. The bond angles to the three nearest neighbors (two As on the upper terrace and one Si on the lower terrace) are $\sim 108^\circ$; i.e., close to the ideal tetrahedral angle of 109.5° . In addition, the fourth electron not bound to the sp^2 -coordinated Si is used to fill the dangling bond, making it a lone pair just as on the As atoms. The resulting electron distribution can be seen in the upper right panel.

For the [$\bar{1}\bar{1}2$] step orientation (see Fig. 4, lower panels), the distortions are even larger. The exposed Si atoms have only two neighbors in the original lattice positions, and they move closer together to form Si-Si bonded pairs. Again, one of the exposed Si atoms retracts into a planar configuration with its neighbors (one As on the upper terrace, the Si of the dimer, and a Si on the lower terrace). Thus it can establish a sp^2 -hybrid electronic configuration, whereas the second Si maintains a sp^3 -hybrid configuration. It binds to three neighbors, and the dangling bond is filled with two electrons, as can be seen in the lower right panel.

The different binding characteristics on the two exposed Si atoms strongly distort the binding angles on the neighboring atoms, and this creates rather strained step geometries with high energies for both orientations.

B. Overhanging As atoms

As can be seen in Fig. 5, the main feature of the steps with overhanging As atoms is the establishment of additional

FIG. 4. Minimum energy structures of steps on Si(111):As with exposed Si atoms with [11 $\bar{2}$] (upper panels) and [$\bar{1}\bar{1}2$] (lower panels) orientation. The left panels show a side view of the atomic arrangement, and the right panels a front view of an isoplane of the electron distribution. One can clearly see the buckling of the Si atoms at the step edge: One Si atom retracts to a planar configuration, forming sp^2 bonds with its three neighbors (for the [11 $\bar{2}$] step two As atoms and one Si atom, for the [$\bar{1}\bar{1}2$] step one As atom and two Si atoms); the other one shows a tetrahedral arrangement with sp^3 bonds and a doubly occupied dangling bond (lone pair) state like the As atoms.

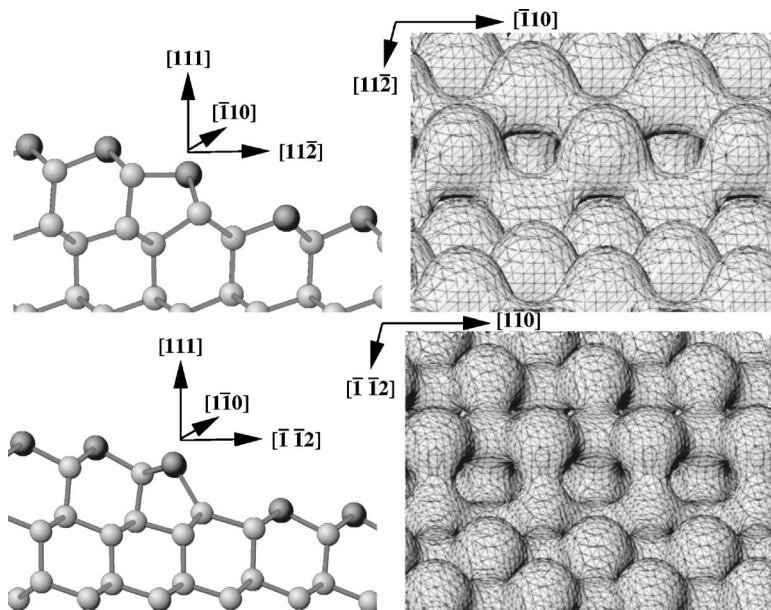


FIG. 5. Minimum energy structure of steps on Si(111):As with overhanging As with $[11\bar{2}]$ (upper panels) and $[\bar{1}\bar{1}2]$ (lower panels) orientation, respectively. The left panels show a side view of the atomic arrangement, and the right panels a front view of an isoplane of the electron distribution. In the left panels, one can clearly see the As binding to the lower terrace Si atoms, yielding a terminating fivefold ring.

bonds of the As atom to lower terrace Si atoms with the formation of a terminating fivefold ring. In the resulting configuration for the $[11\bar{2}]$ step, the extra As atom binds to two Si atoms on the lower terrace and one on the upper one. This results in five bonds for the Si atoms below the overhanging As atoms: three within the double layer and two to overhanging As atoms. All other atoms have ideal coordination number. For the $[\bar{1}\bar{1}2]$ step, all atoms fulfill the bond saturation rule, no Si dangling bonds remain, and all As atoms are binding to three Si neighbors: one on the lower terrace and two on the upper one.

Due to this effect, the bonds in the surface layers of the upper terrace are stretched. The resulting widening of the atom distances decays very slowly with the distance from the step edge. In total, heavily distorted step configurations with high step energies result.

A similar effect has been observed for a Sb-terminated three-layer Ge film on Si(111). There the stretching leads to

an 8% increase of the lateral lattice constant of the film, which is also found experimentally.¹³ This stabilizes the observed (1×1) substructure of the hexagonal islands observed on these Ge films.³⁶

C. Incorporated As atoms

The incorporation of additional As atoms at the terrace edge that replace the exposed Si atoms in the second layer [Fig. 3(c)] yields the lowest energy configurations for both step orientations. Similar to the As coverage on the terrace this replacement avoids any unsaturated Si dangling bonds. The minimum energy configurations are shown in Fig. 6. For the $[11\bar{2}]$ orientation all atoms sit very close to the ideal bulk positions. At these steps, the extra As atoms have their natural threefold coordination, binding to two As atoms on the upper terrace and to one Si atom on the lower one. For the $[\bar{1}\bar{1}2]$ orientation, the bulk-terminated positions of the extra

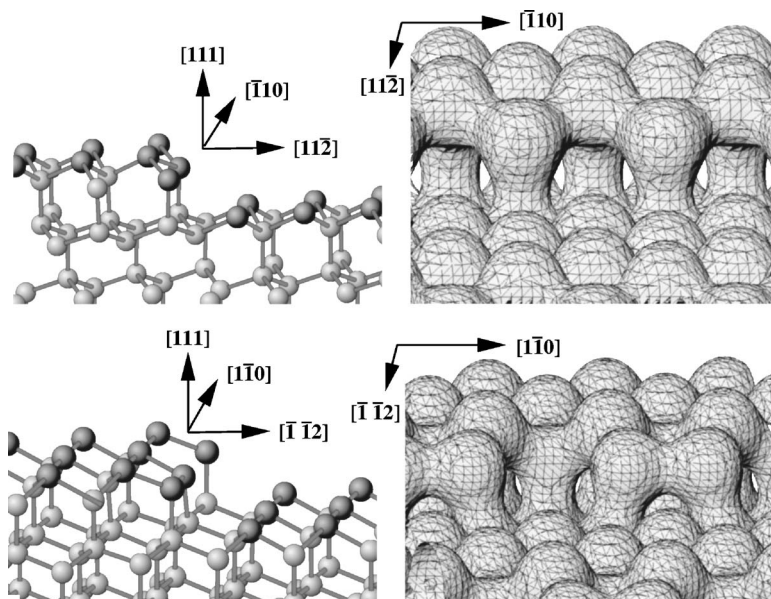


FIG. 6. Minimum energy structure of As-terminated steps on Si(111):As with $[11\bar{2}]$ (upper panels) and $[\bar{1}\bar{1}2]$ (lower panels) orientation. The left panels show a side view of the atomic arrangement, and the right panels a front view of an isoplane of the electron distribution. The characteristic difference in the positions of the As atoms at the step edge in the second layer is clearly visible: nearly ideal bulk termination for the $[11\bar{2}]$ step and As-dimer formation for $[\bar{1}\bar{1}2]$.

As have only two bonds (one bond to an As atom on the upper terrace and one to a Si atom in the lower terrace). These positions are unstable against sideways relaxations, and the As edge atoms form dimers in order to obtain a threefold coordination. This relaxation destroys the ideal bond angles and thus is responsible for the slightly higher energy per unit length of the $[\bar{1}\bar{1}2]$ step.

The incorporation of extra As atoms yields a similar structure at the step edge as the (1×1) terrace structure on As-terminated Si(111). Thus it can easily be imagined that the reactivity of the step edges is reduced in the same way as by the As coverage of the Si(111) terraces: In our previous calculations,³⁷ we have shown that for Ge atoms deposited on Si(111):As surfaces the barrier for incorporation under the As layer is about three times as large as the diffusion barrier on top of the As layer. This is in line with the speculation of Kaxiras^{15–17} concerning the reduced incorporation probability at step edges due to surfactant atoms, especially for Ge adatoms in heteroepitaxy. Indeed, all features of island growth for Si homoepitaxy and Ge heteroepitaxy on Bi-covered Si(111), which differ experimentally with respect to island-distance distribution and island-size distribution, can be recovered in a kinetic Monte-Carlo simulation when one takes into account the very different ratio of the barriers for diffusion and incorporation for Si adatoms (both activation barriers are equal) and for Ge adatoms (the incorporation barrier is three times as high as the diffusion barrier).³⁸

D. Step identification by STM

From the results of the self-consistent electronic structure, one can calculate STM images (simulated STM). According to Tersoff and Hamann³⁹ the tunneling current is proportional to the energy integrated local density of states (LDOS) of the sample at the site of the tip. In order to calculate the LDOS characteristic of the step edges, we first relaxed the surface structure in the way described above. To reduce the coupling of the two surfaces, we enlarged the slab by adding six ideal bulk Si(111) double layers in the middle of the surface relaxed slab, and determined the self-consistent electron structure (without further relaxing the atomic configuration). With the self-consistent electron density, we calculated the wave functions for six special \mathbf{k}_{\parallel} -points out of the irreducible part of the surface Brillouin zone⁴⁰ from which the LDOS of the stepped surface is constructed. We have calculated both the positive- and negative-bias STM images by integrating the surface LDOS over an appropriate energy interval above and below the Fermi energy, respectively.

1. Positive-bias STM

The simulated positive bias STM images, which show the unoccupied states, do not exhibit the calculated distinct differences of the atomic structures of the two step orientations (see Sec. IV C). Due to the antibonding character of the states used for imaging, the resemblance of the atomic structure in the LDOS generated with these states is largely washed out. This can be seen in the simulated STM images in Fig. 7 which are produced with the following parameters: bias voltage +1.0 eV, equi-LDOS plane shown for 2×10^{-8} ,

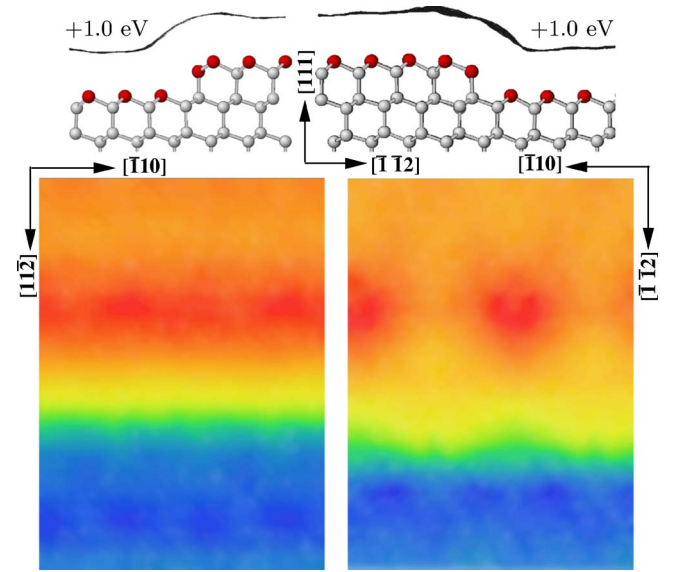


FIG. 7. (Color online) Simulated STM images with positive bias. Shown are the side views (upper panels) and top views (lower panels) of equal-intensity planes of the energy-integrated LDOS ($E_F < \epsilon < E_F + 1.0$ eV) for As-terminated steps with $[11\bar{2}]$ (left panels) and $[\bar{1}\bar{1}2]$ (right panels) orientation, respectively. The corrugation in the STM images does not allow a determination of the atomic structure of the steps. Note the larger distance of the equal-intensity LDOS plane above the As upper terrace atoms next to the step edge in the side views, which resembles the higher brightness in the experimental STM images.

yielding an average distance of the plane from the upper terrace As atoms of ≈ 3.5 Å. In fact, the positive-bias image of the $[11\bar{2}]$ step hardly shows any lateral corrugation along the step, whereas the $[\bar{1}\bar{1}2]$ step exhibits distinct maxima (bright spots) at the upper terrace edge and faint maxima between these spots in front of the step. We will analyze these features in more detail.

There is one common feature in the simulated STM images for positive bias: the enhancement of the LDOS near the upper terrace As atoms next to the step edge. This corresponds to the bright maxima in the experimental STM images (Fig. 2). From the experimental STM image, one cannot decide whether this is due to an elevated position of the As edge atoms or due to an electronic effect. In the *ab initio* structure calculation, we did not find any indication of an outward relaxation of the upper terrace edge atoms. However, compared to the LDOS of As atoms in the middle of the terrace, the LDOS of the edge As atoms shows a clear enhancement in the lower part of the conduction band and a much less pronounced effect at the upper edge of the valence band, as shown in Fig. 8 for the $[\bar{1}\bar{1}2]$ step. Apparently, the LDOS at the conduction band edge of the fundamental gap depends sensitively on the number of As-As bonds: the second layer As atom at the step edge binds to two As atoms (one in the upper terrace and its dimer partner for the $[\bar{1}\bar{1}2]$ step and both in the upper terrace for the $[11\bar{2}]$ step) and has the largest LDOS at the bottom of the conduction band, the upper terrace step edge As binds to one As neighbor and

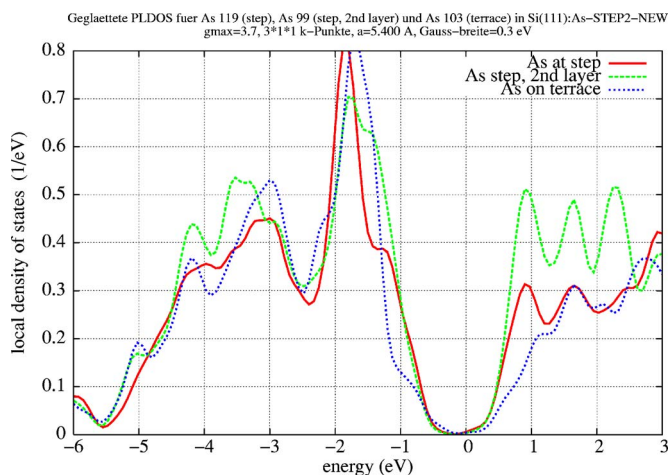


FIG. 8. (Color online) Local density of states of three As atoms for the $[\bar{1}\bar{1}2]$ step: on the upper terrace at the step edge (solid), at step edge, second layer (dashed), and in the middle of the terrace (dotted). The LDOS of the step edge atoms is significantly enhanced in the lower part of the conduction band.

shows the second largest LDOS, and the As atom on the flat terrace has no As neighbor and shows the smallest LDOS. We conclude that the enhancement of the LDOS at the upper terrace As edge atoms is responsible for the brighter maxima in the experimental STM images.

A more detailed analysis shows that the peak structure in the simulated positive bias STM image of the steps is not directly connected to the position of atoms at the edge. For the $[11\bar{2}]$ step, Fig. 7 (left panels) no easily distinguishable maxima show up at the edge, just a “well” (inverted trough) can be seen, with very little structure along the step. This corresponds to a rather unique line scan in the direction perpendicular to the edge, as is seen in our calculated line scan (side view of the LDOS). These line scans for the $[11\bar{2}]$ step for positive bias show a single continuous drop of the LDOS from the upper to the lower terrace.

For the $[\bar{1}\bar{1}2]$ step [Fig. 7 (right panels)], there is only one bright spot in each unit cell, which contains two atoms along

the step. It is actually located in the middle of the triangle formed by three As atoms on the upper terrace (at the T4 site above a second layer Si atom) behind the As edge-atom dimer. The faint additional maxima in front of the step edge are found *between* the bright spots, they are thus located *between* As dimers. This is yet another example that caution has to be exercised when deducing the atomic arrangement from the measured STM images. The line scans for this $[\bar{1}\bar{1}2]$ step orientation show a scatter (across the bright spots and in between) and a double-hump drop from the upper to the lower terrace. However, we found that the line scans for the $[11\bar{2}]$ step orientation are highly sensitive to the bias voltage. For a nominal voltage of +1.5 V, the line scan changes into a “single drop” feature just as for the $[11\bar{2}]$ step. We thus conclude again, that STM images using positive-bias voltage are not well suited for determining the detailed structure of the step edges.

2. Negative-bias STM

While the experimentally available positive bias STM images hardly provide any detailed informations about the atomic configurations at the step edge, we will show that STM images using negative bias would produce a much more detailed picture of the atomic positions at the step edge.

In Fig. 9 the contour lines of the LDOS integrated over the energy range ($E_F - 1.5 \text{ eV} \leq \epsilon \leq E_F$), which resemble the negative bias STM image using occupied states, are shown for the two step orientations considered. As can be seen from the side views in the upper panels, the parameters are chosen to yield simulated STM-images at a tip distance of approximately one Si(111) double layer; i.e., $\approx 3 \text{ \AA}$. According to our experience,⁴¹ this distance is sufficient to yield the asymptotically valid corrugation characteristics.

It is obvious from the top views in the lower panels that the atomic structures of the differently oriented steps can be clearly distinguished. For the $[11\bar{2}]$ orientation the extra As atoms in the second layer are visible as pronounced relative maxima in the middle between the maxima due to the upper terrace As atoms. On the other hand, for the $[\bar{1}\bar{1}2]$ orienta-

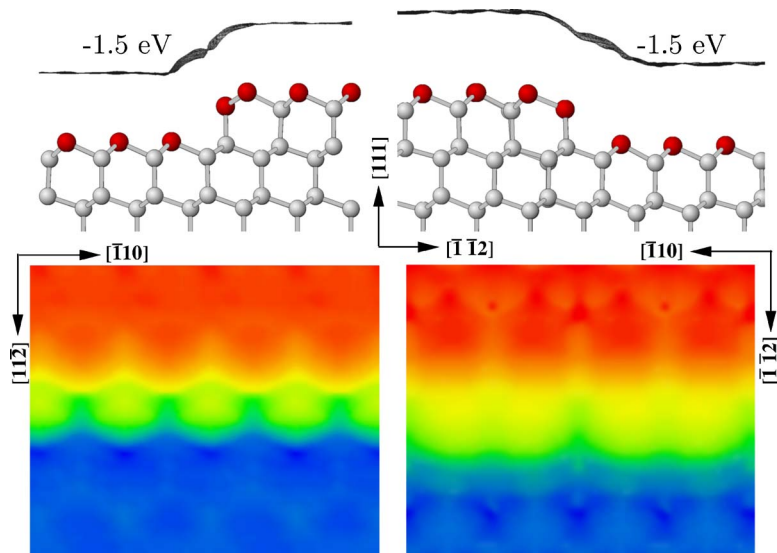


FIG. 9. (Color online) Simulated STM images with negative bias. Shown are the side views (upper panels) and top views (lower panels) of equal-intensity planes of the energy-integrated LDOS ($E_F - 1.5 \text{ eV} < \epsilon < E_F$) for As-terminated steps with $[11\bar{2}]$ (left panels) and $[\bar{1}\bar{1}2]$ (right panels) orientation. In the top-view STM images, the characteristic differences in the positions of the extra As edge atoms in the second layer is clearly visible: nearly ideal bulk termination for the $[11\bar{2}]$ step and As-dimer formation for $[\bar{1}\bar{1}2]$. In the side views, which correspond to experimental line scans, the $[11\bar{2}]$ step shows a more pronounced double hump from the upper to the lower terrace than the $[\bar{1}\bar{1}2]$ step.

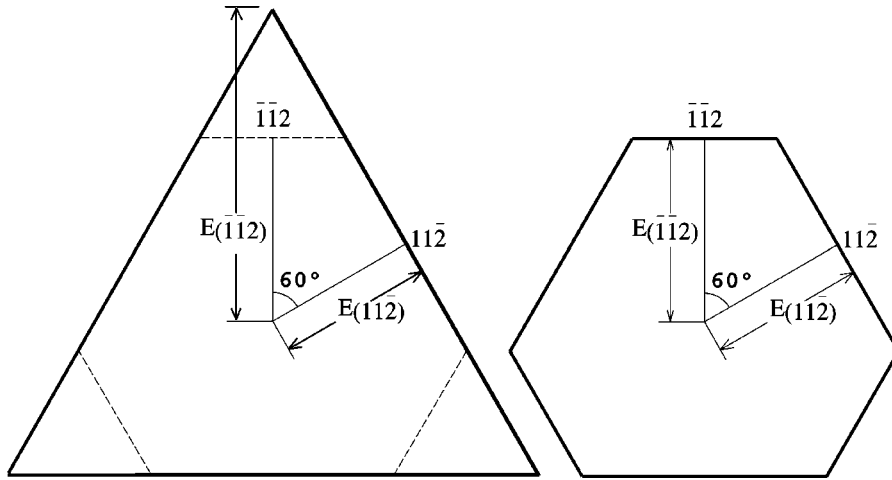


FIG. 10. Wulff plot for the case when only two step orientations are important. The left panel shows a triangular island for the case $E_{[\bar{1}\bar{1}2]} > 2E_{[11\bar{2}]}$, as is expected from the calculated step energies when using As_4 molecules as reference energy for As atoms. The right panel shows the irregular hexagon shape expected from the calculated step energies using bulk As as reference energy for As atoms (see Table II).

tion, the As dimers in the second layer yield slightly washed-out double maxima nearly directly in front of the upper terrace As atom maxima. Note that for negative bias, the equal-intensity LDOS plane does not show extrusions above the As upper-terrace atoms next to the step edge. This is in accordance with the fact that the As-atom LDOS close to the valence band edge shows a much lower sensitivity on the number of As-As bonds than at the conduction band edge (see Fig. 8). Thus, we do not expect pronounced higher brightness spots for these atoms in the experimental negative-bias STM images.

Negative-bias STM images of step-terminated islands on Si(111):As have not yet been reported. Our theoretical results suggest that they are much better suited to determine the orientation and the atomic structure of the steps.

V. EQUILIBRIUM SHAPE OF ISLANDS

In Table II we have collected the calculated step energies for various relaxed configurations. Due to the different numbers of As atoms at the steps (relative to the number of Si atoms, see Table I), the step energies vary linearly with the chemical potential of As. Since the step energies for the As-terminated steps are so much lower than for the other configurations, we can disregard the higher-energy step configurations for the equilibrium considerations, which we are going to discuss now.

The equilibrium shape of As-covered Si islands on Si(111):As can be deduced using a simplified Wulff construction,⁴² where we take into account only the $[11\bar{2}]$ and $[\bar{1}\bar{1}2]$ orientations. This construction is obtained by minimizing the energy of an island as a function of the lengths ℓ_i of the steps with orientation i which have energies ϵ_i per unit length, while keeping the total area A of the island constant. The total step energy is then

$$E_S = \sum_i \epsilon_i \ell_i = \min \quad \text{with } A\{\ell_i\} = \text{const.} \quad (1)$$

According to Wulff,⁴² a point exists inside the island (Wulff's point) such that the distances h_i of steps with orientation i are related to the step energies ϵ_i as

$$\frac{h_i}{\epsilon_i} = \text{const.} \quad (2)$$

In Appendix A we give a short derivation of this relation. In such a construction the distance of a step edge of a particular orientation from the Wulff point is proportional to the edge energy. In the present case of As-covered Si(111), experiments¹⁰ show that only two step orientations are important; namely, $[11\bar{2}]$ and $[\bar{1}\bar{1}2]$ [and those equivalent by symmetry on the hexagonal Si(111) surface]. This selection can be understood on the grounds of bond saturation rules: at other step orientations, the exposed atoms cannot saturate their bonds with a threefold coordination as efficiently; i.e., by moderately large bond distortions. Due to the geometry of the Si(111) surface with threefold symmetry and 60° angles between equivalent $[11\bar{2}]$ and $[\bar{1}\bar{1}2]$ directions and 120° angles between neighboring $[11\bar{2}]$ and $[\bar{1}\bar{1}2]$ directions, we expect triangular or irregular hexagonal islands depending on the relation of the step energies for the two step orientations (see Fig. 10).

Hexagonal islands can only be found in a certain window of the ratio of step energies:

$$\frac{1}{2} < \frac{\epsilon_{[\bar{1}\bar{1}2]}}{\epsilon_{[11\bar{2}]}} < 2. \quad (3)$$

Outside of this range, in a Wulff construction the energetically less favorable step edge would lie outside of the triangle formed by the three energetically more favorable step orientations. The factor of 2 marking the boundaries for the step-energy ratio can be understood from geometrical reasons (see Fig. 10): A hexagon is formed when a corner of the triangle is cut off by the higher-energy step (here $[\bar{1}\bar{1}2]$ orientation). The cutoff triangle is equally sided with two edges formed by the lower-energy step (here $[11\bar{2}]$ orientation) and one edge formed by the higher-energy step. In order that the total step energy (along the circumference of the newly formed hexagon) should be lower than the step energy of the original triangle, the following relations have to hold (assuming $\epsilon_1 < \epsilon_2$):

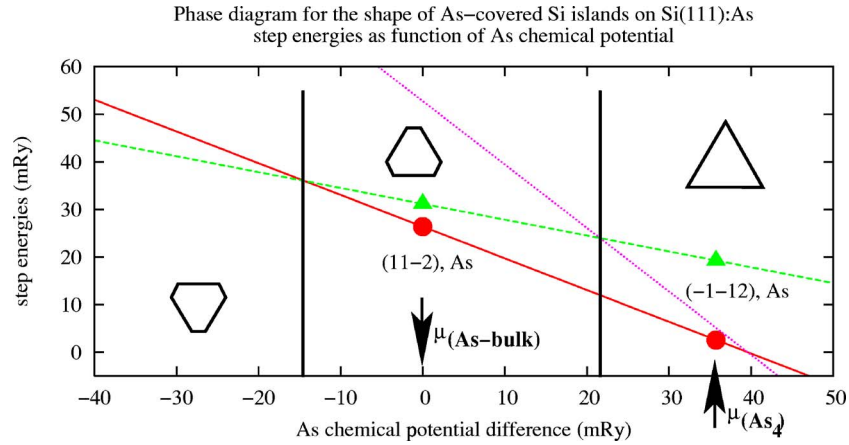


FIG. 11. (Color online) Phase diagram for the equilibrium shape of As-covered Si islands on the Si(111) surface. Lines with data points show the calculated energies for the As-terminated step edges with different orientation (as indicated) as a function of the As chemical potential (relative to As bulk). The dotted line without data points shows twice the energy of the As-terminated steps on Si(111):As with $[11\bar{2}]$ orientation. The vertical lines separate the regions with different island shapes and/or orientation. They are calculated using the variation of the step energies according to Table II and Eq. (3). The accessible range of the As chemical potential between As bulk and As_4 molecules is indicated. With our calculated step energies triangular islands with only $[\bar{1}\bar{1}\bar{2}]$ steps cannot be equilibrium islands.

$$\Delta E_S = \ell_2 \epsilon_2 - 2\ell_2 \epsilon_1 < 0; \quad \epsilon_2 < 2\epsilon_1. \quad (4)$$

From this relation and the variation of the step energies with the As chemical potential (variation of the As reference energy), we can construct a “phase diagram” for the equilibrium shape of As-covered Si islands on the Si(111) surface. This is plotted in Fig. 11, fixing $\mu(\text{As})=0$ at As bulk. The linear dependence of the step energies on the As chemical potential comes from the fact that for the different configurations different numbers of additional As atoms are needed compared to the flat As-terminated terrace. The energy ϵ_i per step length for configuration i is given by

$$\epsilon_i(\mu_{\text{As}}) = \epsilon_i(\mu_{\text{As-bulk}}) - \frac{m_i}{4} \Delta\mu_{\text{As}}, \quad (5)$$

i.e., the slopes of the curves are directly connected with the number m_i of excess As atoms given in the last column of Table I. The extra factor $1/4$ enters because in the unit cells we have chosen there are always four unit lengths of steps (two surfaces, and the basis vector along the step edge having a length of two nearest-neighbor distances). For the phase diagram we have used only the lowest energy step configurations, which are the As-terminated steps for both orientations. The other step configurations not shown in Fig. 11 have excessively high step energies outside of the range of the diagram. One point is worth mentioning: Since the slope of the line for the $[11\bar{2}]$ orientation is twice as large as for the $[\bar{1}\bar{1}\bar{2}]$ orientation, the condition in Eq. (4) never leads to triangular islands with only $[\bar{1}\bar{1}\bar{2}]$ steps in the range for μ_{As} where the step energies are positive. This is true irrespective of the calculated values for the step energy.

From our theoretical results for the step energies, we must conclude that the islands seen in Fig. 1 cannot be equilibrium

islands. The observed length distribution for the two step orientations (also considered theoretically) is opposite to what we would expect for equilibrium islands. In Fig. 1 one sees large islands in the middle of the terrace which have long $[\bar{1}\bar{1}\bar{2}]$ edges and short $[11\bar{2}]$ edges. There are smaller triangular islands, some with only $[\bar{1}\bar{1}\bar{2}]$ edges, but most of them are terminated by $[11\bar{2}]$ edges. On the other hand, in the experimental situation, when As is deposited on the Si(111) surface, one expects growing islands. The larger islands grow at the expense of the shrinking smaller islands. In general, for growing islands the slow growing edge direction will always dominate, whereas for shrinking islands the fast growing edge remains. The only explanation to reconcile the theoretical and experimental results is to speculate that the more stable $[11\bar{2}]$ edges grow so quickly that in a transient state of the growing larger islands they always appear shorter than the less stable $[\bar{1}\bar{1}\bar{2}]$ edges. This is somewhat counter-intuitive but not impossible, since the kinetic stability (growth rate) of an edge is determined by different parameters (activation energies for attachment and detachment of particles) than the edge energies. We conclude that the equilibrium shape of islands still needs experimental verification.

VI. CONCLUSIONS

In conclusion, we have analyzed the atomic structure of terrace steps on Si(111):As. From experimental STM images, *ab initio* calculations, and STM simulations, we can deduce the following: (i) Only step edges with two orientations have been observed to terminate the islands, namely, $[11\bar{2}]$ and $[\bar{1}\bar{1}\bar{2}]$. (ii) The stable edge configurations contain additional As atoms in order to avoid Si dangling bonds. For the $[11\bar{2}]$ step edge orientation, all atom positions are very close to the terminated bulk positions. For the $[\bar{1}\bar{1}\bar{2}]$ orientation, the extra

As atoms form dimers in the second layer to obtain threefold coordination. (iii) Our simulations suggest that in negative-bias STM, which uses the occupied states for imaging, the two differently oriented step edges can clearly be distinguished due to the different atomic arrangements of the second layer As edge atoms. (iv) In the reported positive-bias STM, which uses the unoccupied states for imaging, the determination of the near edge structure or clear distinction of the edge orientation is not possible. The bright spots at near edge atoms on the upper terrace and at island rims are not caused by an elevated position but are due to an increased LDOS in the vicinity of the conduction band edge at these atoms. (v) The theoretically expected equilibrium island shape, irregular hexagons with long edges of $[11\bar{2}]$ orientation, needs experimental verification.

ACKNOWLEDGMENT

The present work was supported by the BMBF Verbundprojekt, Project No.: 22.01D.

APPENDIX

In this appendix we briefly summarize the ideas behind the Wulff construction for the equilibrium shape of a flat island, given the line energies E_i (per unit length) for a discrete set of orientations $i=1\dots N$. The relation derived by G. Wulff⁴² for the equilibrium shape of a three-dimensional crystal can be specified for the two-dimensional case.⁴³ We have to minimize the total step energy E_S [Eq. (1)] for a given area of the island, given by

$$A = \frac{1}{2} \sum_i h_i \ell_i = \text{const}, \quad (\text{A1})$$

where the expression for the area is clear since the total area can be divided into triangles of height h_i and base ℓ_i . Thus, we have to minimize

$$E_S\{h_i\} - \lambda \left(A - \frac{1}{2} \sum_i h_i \ell_i \right) \quad (\text{A2})$$

with respect to a variation of the h_i . λ is a Lagrangian multiplier. A necessary condition for a minimum is

$$0 = \frac{\partial}{\partial h_k} \left(\sum_i \epsilon_i \ell_i - \frac{\lambda}{2} \sum_i h_i \ell_i \right) = \sum_i \left(\epsilon_i - \frac{\lambda}{2} h_i \right) \frac{\partial \ell_i}{\partial h_k} - \frac{\lambda}{2} \ell_k. \quad (\text{A3})$$

We can find a relation between $\frac{\partial \ell_i}{\partial h_k}$ and ℓ_k by observing that for similar islands the step lengths $\ell_k\{h_i\}$ are homogeneous functions of the heights h_i ; i.e., with a scaling factor g , we obtain

$$\ell_k\{gh_i\} = g \ell_k\{h_i\} \quad (\text{A4})$$

Differentiating this equation with respect to g yields

$$\ell_k\{h_i\} = \sum_i h_i \frac{\partial \ell_k}{\partial h_i} = \sum_i h_i \frac{\partial \ell_i}{\partial h_k}. \quad (\text{A5})$$

The last step follows from the existence of the area functional $A\{h_i\}$ [Eq. (A1)]. We thus find

$$\frac{\partial A}{\partial h_i} = \ell_i; \quad \frac{\partial^2 A}{\partial h_i \partial h_k} = \frac{\partial \ell_i}{\partial h_k} = \frac{\partial \ell_k}{\partial h_i}. \quad (\text{A6})$$

Inserting this into Eq. (A3), we obtain

$$0 = \sum_i (\epsilon_i - \lambda h_i) \frac{\partial \ell_i}{\partial h_k}. \quad (\text{A7})$$

On the other hand, by multiplying the right part of Eq. (A3) with h_k and summing over k , we obtain

$$\sum_{i,k} \left(\epsilon_i - \frac{\lambda}{2} h_i \right) h_k \frac{\partial \ell_i}{\partial h_k} = \frac{\lambda}{2} \sum_k h_k \ell_k. \quad (\text{A8})$$

Using Eq. (A5), left part, we finally find

$$\sum_i \epsilon_i \ell_i = \lambda \sum_k h_k \ell_k \quad (\text{A9})$$

The left side of this equation can be identified with the minimum energy $E_{S,\text{min}}$ [Eq. (1)], and the sum on the right side is twice the area of the island [Eq. (A1)]. Thus, we obtain

$$\lambda = \frac{E_{S,\text{min}}}{2A}. \quad (\text{A10})$$

Equation (A7) is a homogeneous system of equations for the variables $(\epsilon_i - \lambda h_i)$, ($i=1\dots N$). However, the determination of the h_i also includes a translation of the Wulff point, which is undetermined by the minimum requirement. Thus, the matrix $\left\{ \frac{\partial \ell_i}{\partial h_k} \right\}$ can only be of rank $(N-2)$, and two degrees of freedom are eliminated by fixing two variables

$$\epsilon_1 - \lambda h_1 = \epsilon_2 - \lambda h_2 = 0; \quad \frac{h_1}{\epsilon_1} = \frac{h_2}{\epsilon_2} = \frac{1}{\lambda}. \quad (\text{A11})$$

From Eq. (A7), it is obvious that a solution can be obtained by setting all variables $(\epsilon_i - \lambda h_i)$ to zero, which yields

$$\frac{h_i}{\epsilon_i} = \frac{1}{\lambda}; \quad i = 1 \dots N. \quad (\text{A12})$$

This is Wulff's construction [Eq. (2)]. Dinghas⁴⁴ has proved that this solution indeed yields the shape of the island with minimal energy.

The minimal energy shape is independent of the size of the islands if discrete lattice effects and effects of island corners can be neglected. This should be the case for islands which are terminated by steps with lengths large compared to the lattice constant.

The factor $1/\lambda$ is a scaling factor for the Wulff distances h_i . Due to the similarity of the islands also the step lengths ℓ_i are proportional to $1/\lambda$. This means that the area A of the islands [Eq. (A1)] scales as $1/\lambda^2$, and the energy E_S [Eq. (1)] as $1/\lambda$. Thus, E_S^2/A is independent of the size of the islands for similar islands constructed according to Eq. (A12). It is a function of the shape only.

- ¹*Nanoelectronics and Information Technology: Advanced Electronic Materials and Novel Devices*, edited by R. Waser (Wiley-VCH, Weinheim, 2003).
- ²S. M. Sze, *Modern semiconductor Device Physics* (Wiley, New York, 1998).
- ³M. Copel, M. C. Reuter, E. Kaxiras, and R. M. Tromp, Phys. Rev. Lett. **63**, 632 (1989); M. Copel, M. C. Reuter, M. HornvonHoegen, and R. M. Tromp, Phys. Rev. B **42**, 11682 (1990).
- ⁴C. Y. Fong, M. D. Watson, L. H. Yang, and S. Ciraci, Modell. Simul. Mater. Sci. Eng. **10**, R61 (2002).
- ⁵M. Horn-vonHoegen, F. K. LeGoues, M. Copel, M. C. Reuter, and R. M. Tromp, Phys. Rev. Lett. **67**, 1130 (1991).
- ⁶G. Meyer, B. Voigtländer, and N. M. Amer, Surf. Sci. **274**, L541 (1992).
- ⁷B. Voigtländer and A. Zinner, J. Vac. Sci. Technol. A **12**, 1932 (1994).
- ⁸T. Schmidt, J. Falta, G. Materlik, J. Zeysing, G. Falkenberg, and R. L. Johnson, Appl. Phys. Lett. **74**, 1391 (1999).
- ⁹D. Reinking, M. Kammler, N. Hoffmann, M. Horn-von Hoegen, and K. R. Hofmann, Electron. Lett. **35**, 503 (1999).
- ¹⁰B. Voigtländer, A. Zinner, Th. Weber, and H. P. Bonzel, Phys. Rev. B **51**, 7583 (1995).
- ¹¹K. Schroeder, B. Engels, P. Richard, and S. Blügel, Phys. Rev. Lett. **80**, 2873 (1998).
- ¹²M. Horn-von Hoegen, Z. Kristallogr. **214**, 591 (1999); **214**, 684 (1999).
- ¹³N. Theuerkauf, Ph.D. thesis, RWTH, Aachen, 1999.
- ¹⁴A. Antons, K. Schroeder, B. Voigtländer, V. Cherepanov, R. Berger, and S. Blügel, Phys. Rev. Lett. **89**, 236101 (2002).
- ¹⁵E. Kaxiras, Mater. Sci. Eng., B **30**, 175 (1995).
- ¹⁶D. Kandel and E. Kaxiras, Phys. Rev. Lett. **75**, 2742 (1995).
- ¹⁷D. Kandel, Phys. Rev. Lett. **78**, 499 (1997).
- ¹⁸J. S. Ha, K-H. Park, Y-J. Ko, and K. Park, J. Vac. Sci. Technol. B **20**, 747 (2002).
- ¹⁹T. Sekiguchi, S. Yoshida, and K. M. Itoh, Phys. Rev. Lett. **95**, 106101 (2005).
- ²⁰R. M. Feenstra and J. A. Stroscio, Phys. Rev. Lett. **59**, 2173 (1987).
- ²¹P. Segovia, D. Purdie, M. Hengsberger, and Y. Baer, Nature (London) **402**, 504 (1999).
- ²²R. Losio, K. N. Altmann, A. Kirakosian, J.-L. Lin, D. Y. Petrovykh, and F. J. Himpsel, Phys. Rev. Lett. **86**, 4632 (2001).
- ²³I. K. Robinson, P. A. Bennett, and F. J. Himpsel, Phys. Rev. Lett. **88**, 096104 (2002).
- ²⁴D. Sanchez-Portal and R. M. Martin, Surf. Sci. **532–535**, 655 (2003).
- ²⁵C. Gonzalez, P. C. Snijders, J. Ortega, R. Perez, F. Flores, S. Rogge, and H. H. Weitering, Phys. Rev. Lett. **93**, 126106 (2004).
- ²⁶P. C. Snijders, S. Rogge, C. Gonzalez, R. Perez, J. Ortega, F. Flores, and H. H. Weitering, Phys. Rev. B **72**, 125343 (2005).
- ²⁷M. A. Olmstead, R. D. Bringans, R. I. G. Uhrberg, and R. Z. Bachrach, Phys. Rev. B **34**, 6041 (1986).
- ²⁸P. Martensson, G. Meyer, N. M. Amer, E. Kaxiras, and K. C. Pandey, Phys. Rev. B **42**, 7230 (1990).
- ²⁹J. Falta, T. Schmidt, G. Materlik, J. Zeysing, G. Falkenberg, and R. L. Johnson, Appl. Surf. Sci. **162–163**, 256 (2000).
- ³⁰B. Voigtländer, Surf. Sci. Rep. **43**, 127 (2001).
- ³¹R. Berger, S. Blügel, A. Antons, Wi. Kromen, and K. Schroeder, *NIC-Workshop “Molecular Dynamics on Parallel Computers”* (World Scientific, Singapore, 2000), p. 185.
- ³²L. Kleinman and D. M. Bylander, Phys. Rev. Lett. **48**, 1425 (1982).
- ³³S. H. Vosko, L. Wilk, and M. Nusair, Can. J. Phys. **58**, 1200 (1980).
- ³⁴R. Fletcher, *Practical Methods of Optimization* (John Wiley & Sons, New York, 1987).
- ³⁵Tests show that the atomic configurations do not change much ($\Delta d < 0.05 \text{ \AA}$) with the size of the basis set when varying the cutoff energy from 9 to 13.69 Ry. The estimated error for calculated energy differences is approximately 0.05 eV. For the calculation of the theoretical STM images (local density of states) we used an enlarged slab, a cutoff of 13.69 Ry, and the appropriate theoretical lattice constant of 5.40 Å.
- ³⁶A. Antons, Y. Cao, B. Voigtländer, K. Schroeder, R. Berger, and S. Blügel, Europhys. Lett. **62**, 547 (2003).
- ³⁷K. Schroeder, A. Antons, R. Berger, and S. Blügel, Phys. Rev. Lett. **88**, 046101 (2002).
- ³⁸V. Cherepanov, S. Filimonov, J. Myslivecek, and B. Voigtländer, Phys. Rev. B **70**, 085401 (2004).
- ³⁹J. Tersoff and D. R. Hamann, Phys. Rev. B **31**, 805 (1985).
- ⁴⁰S. Heinze, S. Blügel, R. Pascal, M. Bode, and R. Wiesendanger, Phys. Rev. B **58**, 16432 (1998).
- ⁴¹B. Engels, P. Richard, K. Schroeder, S. Blügel, Ph. Ebert, and K. Urban, Phys. Rev. B **58**, 7799 (1998).
- ⁴²G. Wulff, Z. Kristallogr. **34**, 449 (1901).
- ⁴³M. von Laue, Z. Kristallogr. **105**, 124 (1943).
- ⁴⁴A. Dinghas, Z. Kristallogr. **105**, 304 (1943).